Taylor & Francis
Taylor & Francis Group

Spectroscopy Letters

An International Journal for Rapid Communication

ISSN: 0038-7010 (Print) 1532-2289 (Online) Journal homepage: http://www.tandfonline.com/loi/lstl20

High–pressure electrical conductivity and Raman spectroscopy of chalcanthite

Chang Pu, Lidong Dai, Heping Li, Haiying Hu, Yukai Zhuang, Kaixiang Liu, Linfei Yang & Meiling Hong

To cite this article: Chang Pu, Lidong Dai, Heping Li, Haiying Hu, Yukai Zhuang, Kaixiang Liu, Linfei Yang & Meiling Hong (2018): High–pressure electrical conductivity and Raman spectroscopy of chalcanthite, Spectroscopy Letters, DOI: 10.1080/00387010.2018.1522646

To link to this article: https://doi.org/10.1080/00387010.2018.1522646

Published online: 06 Dec 2018.

SPECTROSCOPY LETTERS
https://doi.org/10.1080/00387010.2018.1522646

High–pressure electrical conductivity and Raman spectroscopy of chalcanthite

Chang Pu[a,b], Lidong Dai[a], Heping Li[a], Haiying Hu[a], Yukai Zhuang[a,b], Kaixiang Liu[a,b], Linfei Yang[a,b], and Meiling Hong[a,b]

[a]Key Laboratory of High Temperature and High Pressure Study of the Earth's Interior, Institute of Geochemistry Chinese Academy of Sciences, Guiyang, Guizhou, China; [b]University of Chinese Academy of Sciences, Beijing, China

ABSTRACT

The phase transitions and dehydration of chalcanthite were investigated by electrical conductivity and Raman spectroscopy at 1.0–24.0 GPa and 293–673 K in a diamond anvil cell. At ambient temperature, two secondary phase transitions were observed according to discontinuous changes in the slope of Raman shifts, full width at half maximum and electrical conductivities at ~7.3 and ~10.3 GPa. The dehydration temperatures were determined by the splitting of Raman peaks and changes in electrical conductivity as ~350 and ~500 K at respective ~3.0 and ~6.0 GPa. A positive relationship for chalcanthite between dehydration temperature and pressure is established.

ARTICLE HISTORY
Received 13 March 2018
Accepted 9 September 2018

KEYWORDS
chalcanthite; dehydration; electrical conductivity; phase transition; Raman spectroscopy

Introduction

Chalcanthite (copper sulfate pentahydrate), a well–known hydrous sulfate, belongs to the chalcanthite group of minerals. As a widely accepted standard test molecule, copper sulfate pentahydrate is frequently used as a calibration material for quantitative water desorption or decomposition studies.[1] At ambient pressure, chalcanthite crystallizes in the triclinic structure. The parameters of the chalcanthite unit cell are $a = 6.141$ Å, $b = 10.736$ Å, and $c = 5.968$ Å, and $\alpha = 82°$, $\beta = 107°$ and $\gamma = 102°$.[2] The relationships between all the atoms can be described as follows. There are two types of the water molecule in the crystal structure. The first type, of which there are four, are attached to a copper atom in a square plane by coordination bonds. The second type is linked to two coordinated water molecules and a sulfate anion by hydrogen bonding. The Cu–O bond connected to SO_4^{2-} is perpendicular to the square plane. Unlike the cases for other sulfates or phosphates, SO_4^{2-} loses its tetrahedral symmetry to form an infinite chain, i.e., H_2O–Cu–SO_4^{2-}–Cu–H_2O.[3,4]

The high–pressure phase stability of hydrous sulfate minerals at room temperature has attracted considerable attention due to some pressure–induced variations of the vibrational spectroscopic and ultrasonic elastic wave properties in the past several years. Some researchers discovered the occurrence of phase transitions for gypsum ($CaSO_4 \cdot 2H_2O$) at ~4.4, ~8.5, and ~10.8 GPa on the basis of Raman spectroscopy and X-ray diffraction observations.[5] Brand et al.[6] found that mirabilite ($Na_2SO_4 \cdot 10H_2O$) underwent structural reorganizations at ~7.5 and ~20.0 GPa by theoretical calculations. More recently, Gromnitskaya et al.[7] investigated the pressure–induced phase transitions of epsomite ($MgSO_4 \cdot 7H_2O$) by ultrasonic and neutron powder diffraction and found the transformations occurred at ~1.4, ~1.6, and ~2.5 GPa and 280–295 K. It implied that hydrous chalcanthite may undergo similar phase transitions at high pressure and room temperature. However, the structural and vibrational properties of chalcanthite were mainly investigated at atmospheric pressure. Previous X-ray diffraction and neutron–diffraction studies have determined the structural information of chalcanthite from room temperature to 363 K and ambient pressure.[2,8–10] Raman spectroscopic studies on the assignments for each vibrational mode of chalcanthite were carried out at the temperature range from 95 to 298 K and atmospheric pressure.[3,11,12] To our knowledge, the high–pressure phase stability of chalcanthite has not been reported at room temperature till now.

As we know, in general, hydrous mineral and rock will dehydrate at high temperature and high-pressure conditions. In order to clearly describe the dehydration process, many researchers have tried to establish the phase diagram of dehydration temperature and pressure by comparing the variation of physical parameters before and after dehydration. However, the relationship between dehydration temperature and pressure for hydrous minerals and rocks remains controversial till now. Some researchers think that a negative correlation between dehydration temperature and pressure for the hydrous phyllite has been acquired according to high–temperature and high–pressure electrical conductivity measurements.[13] On the other hand, a positive correlation of dehydration temperature and the pressure was established for hydrous pyrophyllite ($Al_2Si_4O_{10}(OH)_2$) and gypsum ($CaSO_4 \cdot 2H_2O$) by electrical conductivity and

CONTACT Lidong Dai dailidong@gyig.ac.cn Key Laboratory of High Temperature and High Pressure Study of the Earth's Interior, Institute of Geochemistry Chinese Academy of Sciences, Guiyang, Guizhou 550081, China.
Color versions of one or more of the figures in the article can be found online at www.tandfonline.com/lstl.

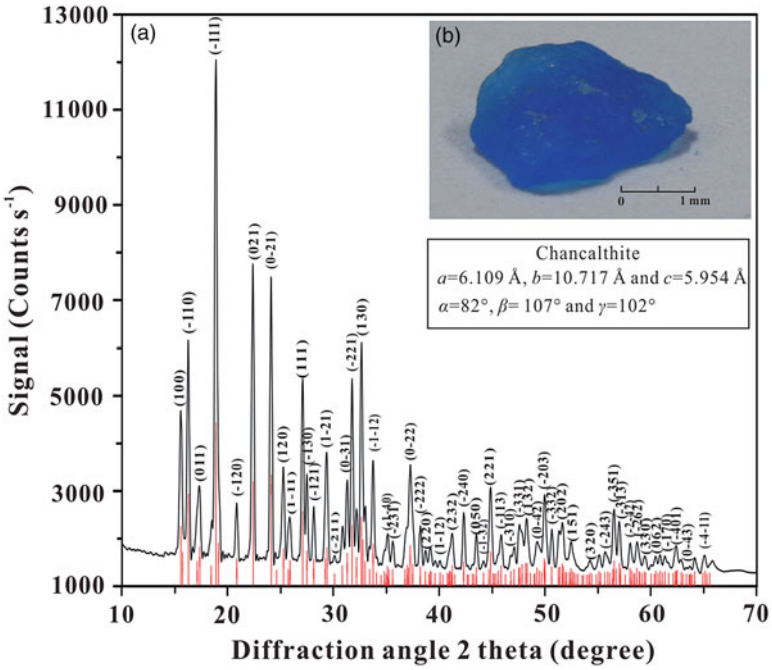

Figure 1. (a) The X–ray diffraction pattern and picture of natural sample of chalcanthite. The figure reveals that the starting sample was pure by good agreement with the standard data for pure chalcanthite (Operating conditions: working voltage 40 kV; working current 40 mA.) (b) The picture of natural sample of chalcanthite.

differential pressure analysis, respectively.[14,15] Whereas, in order to explore the dehydration process, most of the previously available work for hydrous chalcanthite was completed under conditions of high temperature and room pressure. A discontinuous variation of electrical conductivity on the hydrous chalcanthite at ~383 K was performed to extrapolate the occurrence of dehydration reaction under the atmospheric pressure.[16] Chang and Huang[17] observed that the dehydration from chalcanthite to bonattite ($CuSO_4{\cdot}3H_2O$) occurred at 352 K by high–temperature Raman spectroscopy at atmospheric pressure. Similar IR spectroscopy and temperature dependent desorption mass spectrometry results also confirmed that the dehydration reaction (chalcanthite–bonattite) appeared at a temperature range from 333 K to 373 K at ambient pressure.[1,18] However, as a representative of hydrous mineral, there are no reports of phase changes as a function of dehydration temperature and pressure in copper sulfate pentahydrate.

In this study, a series of Raman scattering and electrical conductivity experiments on chalcanthite were performed at pressures up to ~24.0 GPa and temperatures up to 673 K, using a diamond anvil cell (DAC). Two-phase transitions were observed at high pressure and room temperature. A correlation between dehydration temperature and pressure for chalcanthite is established in a wide temperature and pressure range.

Experimental

Natural chalcanthite was collected from the Hongtoushan deposit, Liaoning Province in northeast China. It was formed in the oxidation zones of deposits at the post-mining formation stage, and the oxidation zone can be affected by surface water, which is saturated with copper and acidic ions. Single crystals without visible impurities were selected for the experiments. The samples were cleaned with ethanol and acetone. The X-ray diffraction pattern of the starting material is shown in Fig. 1(a). The data analysis and handling software JADE 6.0 was used. The lattice parameters are $a = 6.109$ Å, $b = 10.717$ Å, and $c = 5.954$ Å; $\alpha = 82°$, $\beta = 107°$, and $\gamma = 102°$. The unit cell volume is 362.16 Å^3. These values correspond to those for a pure chalcanthite single crystal.[2] The observed XRD peaks are in good agreement with the standard data for pure chalcanthite. Figure 1(b) shows a photograph of the chalcanthite sample. The gel–class chalcanthite single crystals are blue and the grain size is nearly 3.0 mm. The samples were ground to powders in an agate mortar before the high-temperature and high-pressure experiments.

A diamond anvil cell with an anvil culet of size 300 μm was used for high-temperature and high-pressure electrical conductivity and Raman spectroscopy measurements. Two external resistance heating furnaces were placed around upper and lower diamond anvils to provide high-temperature conditions. During the experiments, no extra pressure medium was added. Before sample loading, a T–301 stainless–steel gasket was pre–indented to a thickness of 40 μm and a hole of size 200 μm was made with a laser. For the electrical conductivity measurements, a mixture of boron nitride powder and epoxy resin were crushed into the hole and another hole of size 100 μm was drilled to form an insulating sample chamber at the center. During the measurements, the diamond anvil was used for pressure calibration. Figure 2 shows a diagram of the diamond anvil cell used in the experiments. AC impedance spectroscopy was performed with an impedance spectrometer (1260, Solartron) with a dielectric interface (1296, Solartron) at frequencies of

10^{-1}–10^{7} Hz. A plate electrode was integrated into both diamond anvils. A *K*–type thermocouple with an estimated accuracy of 5 K was directly bonded to one side of the diamond anvil for temperature measurements. The specific measurement procedure is described in previous reports.[19,20]

High-pressure Raman spectroscopy was performed with the same DAC. Unlike the case for the electrical measurements, a tiny ruby was added to the sample chamber for pressure calibration. In the high-temperature and high-pressure experiments, the pressure was fixed at a certain value and the temperature was increased up to 673 K. Raman spectra were collected using a Raman spectrometer (Invia, Renishaw, UK) equipped with a confocal microscope (TCS SP8, Leica, Germany) and a CCD camera (Olympus). The typical excitation laser power was ~20 mW for Raman spectroscopy and 0.5–40 μW for fluorescence spectroscopy. Spectra were recorded in the backscattering geometry using an argon ion laser (Spectra physics; 514.5 nm and power <1 mW) in the range of 100–1200 and 2800–3800 cm^{-1} with a spectral resolution of 1.0 cm^{-1}. Each acquisition lasted for 120 s. The results were fitted with PeakFit software (China). Some available high-pressure overlapping Raman band locations and widths were determined by using PeakFit Gaussian curve fitting software (China). Detailed descriptions of the high-pressure Raman experimental procedures can be found elsewhere.[21,22]

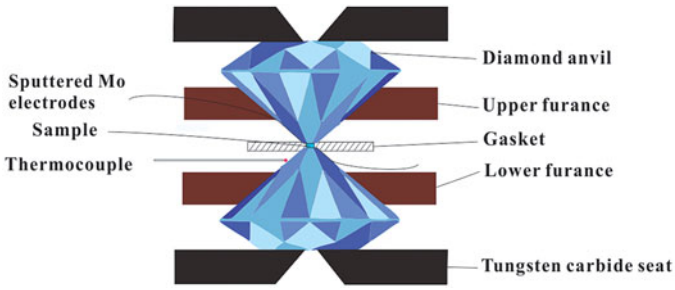

Figure 2. Experimental assembly for electrical conductivity measurement.

Results and discussion

Raman spectroscopy of chalcanthite at high pressure

Some of the primary Raman peaks of chalcanthite observed during compression at room temperature are shown in Fig. 3. The Raman modes of chalcanthite can be roughly divided into four areas. (1) Frequency shifts in the range 3000–3600 cm^{-1}, which corresponds to the internal modes of H_2O. The peaks at 3221 and 3362 cm^{-1} corresponds to the ν_1 (H_2O) and ν_3 (H_2O) modes, respectively. (2) The Raman shifts in the range 450–1200 cm^{-1} correspond to the vibrational modes of SO_4^{2-}. The ν_1 (SO_4) mode (983 and 1057 cm^{-1}), ν_2 (SO_4) mode (460 cm^{-1}), ν_3 (SO_4) mode (1144 and 1100 cm^{-1}), and ν_4 (SO_4) mode (610 cm^{-1}) are observed in the Raman spectra at 1.6 GPa. (3) The peaks in the range 200–450 cm^{-1} correspond to the vibrational mode of the Cu–O bond (429, 330, and 249 cm^{-1}). (4) The peaks in the range 100–200 cm^{-1} are related to lattice modes. These results are generally consistent with those of previous studies at atmospheric pressure.[17,23–26] Figure 3(a) shows that the Raman modes of SO_4^{2-} exhibited blue shifts and weakened with increasing pressure. As the pressure was released to atmospheric pressure, the original Raman spectrum of SO_4^{2-} was recovered, except for a slight change in the intensity. Figure 3(b) shows the Raman spectra for H_2O at room temperature and pressures up to ~23.5 GPa. Two obvious Raman peaks are observed at 3221 and 3362 cm^{-1}, which corresponds to the ν_1 (H_2O) and ν_3 (H_2O) vibrational modes, with A_1 and B_1 symmetry, respectively. On compression, the peaks at 3221 and 3362 cm^{-1} moved to the lower and higher frequency ranges, respectively, the ν_1

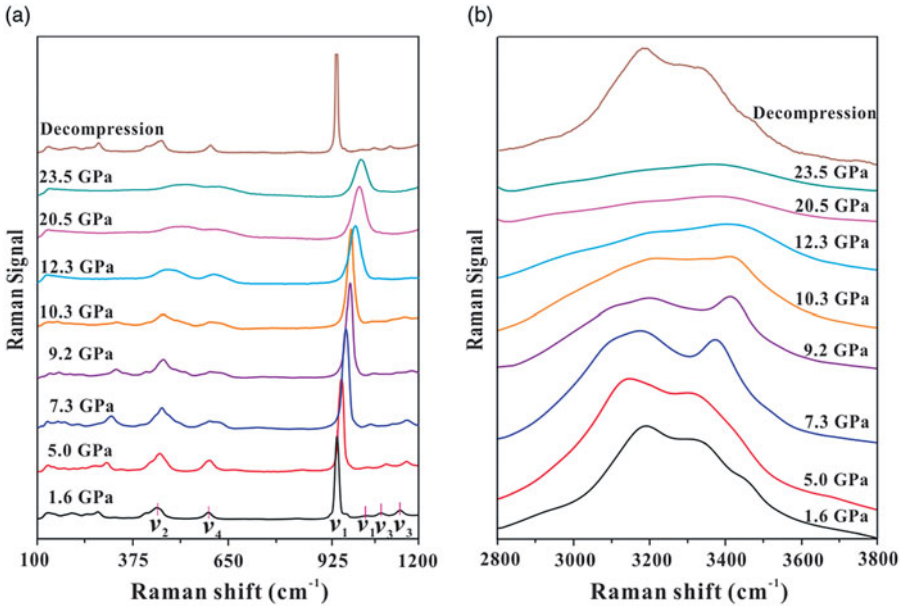

Figure 3. Raman spectroscopic results of chalcanthite at the pressure range of 1.6–23.5 GPa and room temperature. The variation of the vibrational modes of (a) sulfate anion and (b) water molecule. (Operating conditions: excitation laser power 20 mW.) GPa–pressure (gigapascal) and ν_1, ν_2, ν_3, and ν_4–four vibrational modes of sulfate anion.

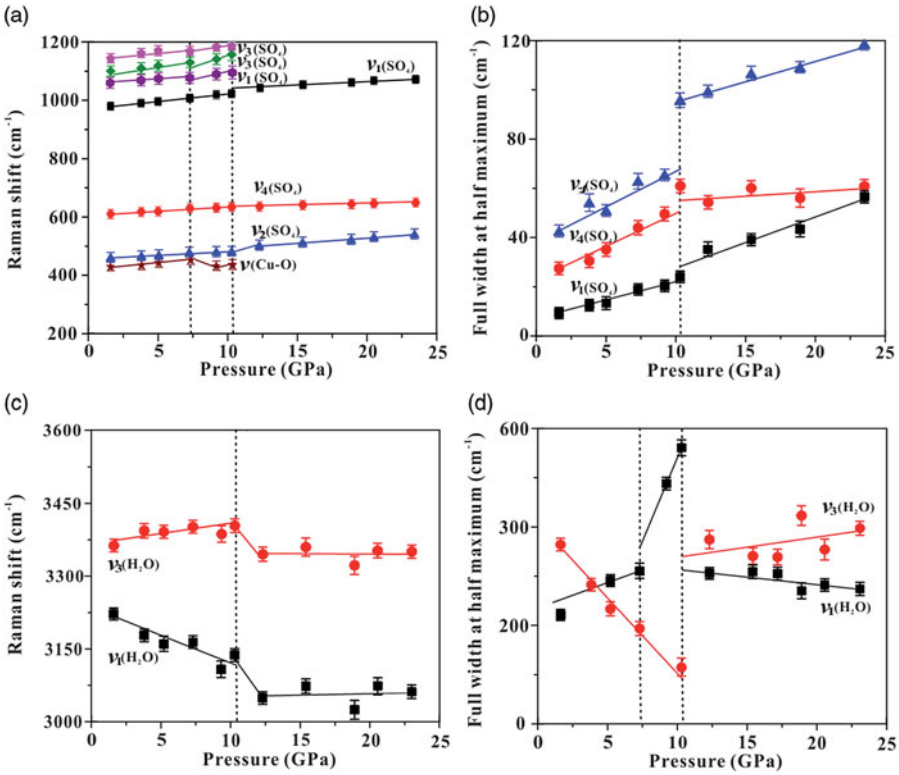

Figure 4. Raman spectra of chalcanthite at 1.6–23.5 GPa and room temperature. (a) and (c) The variations of Raman mode frequency against pressure. (b) and (d) Raman full width at half maximum for vibrational modes with increasing pressure. ν_1 (SO_4), ν_2 (SO_4), ν_3 (SO_4), and ν_4 (SO_4)–four vibrational modes of sulfate anion; ν (Cu–O)–vibrational mode of Cu–O bond and ν_1 (H_2O) and ν_3 (H_2O)–vibrational modes of water molecule.

(H_2O) peak gradually broadened, and the ν_3 (H_2O) peak became increasingly intense. When the pressure was removed, the Raman spectrum reverted to the original shape under ambient conditions.

Generally, a pressure-induced phase transition is accompanied by a corresponding variation in the full width at half maximum (FWHM).[27] Figure 4(a) shows the linear relationship between pressure and the Raman shift. For the ν_1 (SO_4) (1057 cm^{-1}) and ν (Cu–O) modes, discontinuities of slope occurred at 7.3 GPa. For the ν_4 (SO_4) mode, it appeared to shift continuously with pressure, but a calculation showed that the slope for the ν_4 (SO_4) mode had an inflection point at 7.3 GPa and changed from 2.6 to 1.3. The peaks for the ν (Cu–O), ν_1 (SO_4) (1057 cm^{-1}) and ν_3 (SO_4) (1100 and 1144 cm^{-1}) Raman modes disappeared when the pressure was increased to 10.3 GPa. An obvious discontinuity of slope for the ν_2 (SO_4) mode was also observed at 10.3 GPa. Figure 4(b) shows that the linear relationship between the FWHM and pressure clearly broke down at 10.3 GPa for the ν_2 (SO_4), and ν_4 (SO_4) Raman modes. Figures 4(c,d) show that the ν_1 (H_2O) and ν_3 (H_2O) peaks exhibited a red shift and blue shift, respectively, and then changed slightly after 10.3 GPa. The pressure dependence of the FWHM of ν_1 (H_2O) and ν_3 (H_2O) also showed two clear discontinuity points, at 7.3 and 10.3 GPa.

In our present work, all these observations regarding ν_1 (SO_4) at 1057 cm^{-1}, ν_2 (SO_4) at 460 cm^{-1}, ν_3 (SO_4) at 1100 and 1144 cm^{-1}, ν (Cu–O) at 420 cm^{-1}, and the vibrational modes of H_2O indicate the occurrence of phase transitions. However, variations in ν_1 (SO_4) at 983 cm^{-1} and the ν_4 (SO_4) Raman modes are not obvious at 7.3 and 10.3 GPa. The discontinuities in the slopes of the frequency versus pressure and FWHM versus pressure plots show that the bonding forces among all the atoms were changed by high pressure, i.e. the bonds in the crystal were adjusted and reset on compression. The vibrational modes of SO_4^{2-} were likely to be influenced by relative changes in the Cu–O bond when chalcanthite was compressed. There were no new peaks or peak splitting below ~24.0 GPa, therefore, it was deduced that the SO_4^{2-} tetrahedron was not completely destroyed, the overall chalcanthite structure had a new orientation symmetry. For the vibrational modes of H_2O, volume compression can enhance hydrogen bonding, which may lead to the differences between the behaviors of ν_1 (H_2O) and ν_3 (H_2O) modes when phase transitions occur.[28] In the present study, Raman scattering experiment on the sample was performed at pressures up to a maximum value of ~24.0 GPa, but this pressure was not high enough to completely destroy the original crystalline structure. The Raman spectrum, therefore, recovered when the pressure was removed, which implies that this high-pressure phase transition is also reversible.

Impedance spectroscopy of chalcanthite at high pressure

Pressure-induced electrical conductivity measurements were performed at room temperature, the impedance spectra in the range 1.4–24.2 GPa are shown in Figs. 5(a,b).

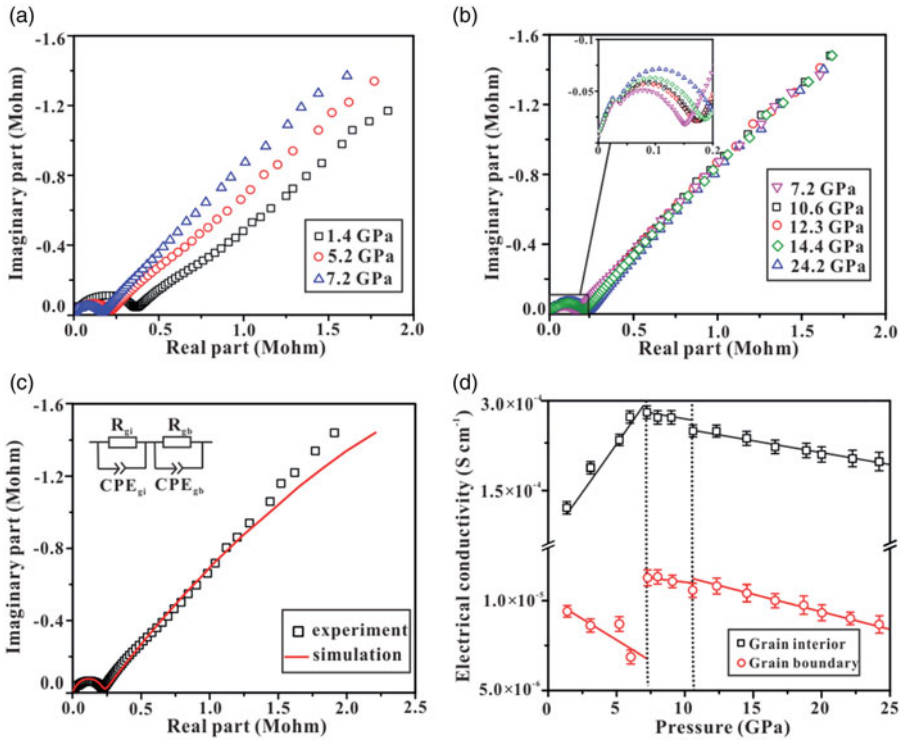

Figure 5. Selected impedance spectroscopy of chalcanthite at the pressure range from 1.4 to 24.2 GPa and ambient temperature. (a) and (b) Impedance spectra of chalcanthite at 1.4–24.2 GPa, (c) a typical fitted impedance spectroscopy of chalcanthite using the equivalent circuit at 5.2 GPa and (d) pressure dependence of electrical conductivity of chalcanthite. (Operating conditions: signal voltage 1 V; scanning frequency range 10^{-1} to 10^{7} Hz.). *R*–resistance; CPE–constant phase element; gi–grain interior; gb–grain boundary and S–(Siemens).

The impedance spectra data were fitted with ZView software to an equivalent circuit (UK). The impedance spectroscopy can be divided into two parts, namely a semi-circular arc in the high-frequency region, which represents grain interior conductivity, and an oblique line in the low-frequency region, which corresponds to grain boundary conductivity. The equivalent circuit contains two units, which are composed of R_{gi}–CPE_{gi} and R_{gb}–CPE_{gb} in series (*R* and CPE represent the resistance and constant phase element, respectively; the subscripts gi and gb denote grain interior and grain boundary, respectively). The electrical conductivities of the samples were calculated as follows:

$$\sigma = (1/R) \times (l/A) \quad (1)$$

where σ is the electrical conductivity, and A and l are the electrode area and the distance between the two electrodes, respectively. To verify deviation from the equivalent circuit, one typical impedance spectroscopy and its corresponding fitting curve at 5.2 GPa are shown in Fig. 5(c).

Figure 5(d) shows the pressure dependences of the grain interior conductivity and grain boundary conductivity during compression. The grain interior electrical conductivity (σ_{gi}) increases with increasing pressure, whereas the grain boundary electrical conductivity (σ_{gb}) shows the opposite trend at pressures below 7.2 GPa. At pressures above 7.2 GPa, the grain interior electrical conductivity and the grain boundary electrical conductivity both decrease with increasing pressure. Linear fitting clearly shows that the variations in the slope of the pressure versus electrical conductivity plot are divided into two parts by an inflection point at 7.2 GPa. The available discontinuities of the electrical conductivity at 7.2 GPa can be attributed to pressure-induced phase transitions, this is consistent with the Raman scattering observations. However, the occurrence of a phase transition at ~10 GPa is not clear from the relationship between the electrical conductivity and pressure, as shown in Fig. 5(d). It is possible that, to some degree, some physical parameters are not sensitive to reveal the occurrence of the phase transition. Therefore, a combination of the Raman scattering and electrical conductivity measurements was used to analyze the phase transitions. The Raman spectra clearly indicate two phase transitions, at ~7.3 and ~10.3 GPa, whereas the graph of the pressure dependence of the electrical conductivity shows only one clear phase transition, at ~7.3 GPa.

A combination of our obtained Raman spectra and electrical conductivity measurements shows one observable change in the electrical conductivity and two clear discontinuities in the pressure-dependent Raman shifts and FWHM rather than the splitting phenomena or the appearance of new peaks in the Raman spectra. The transformations of the entire structure are reversible at atmospheric temperature. On the basis of these results, it can be deduced that two secondary phase transitions occurred.

Raman spectroscopy of chalcanthite at high pressure and high temperature

The Raman spectra for the SO_4^{2-} vibrational modes at 2.9 GPa and 293–423 K are shown in Fig. 6(a). The Raman modes changed smoothly at room temperature to 353 K.

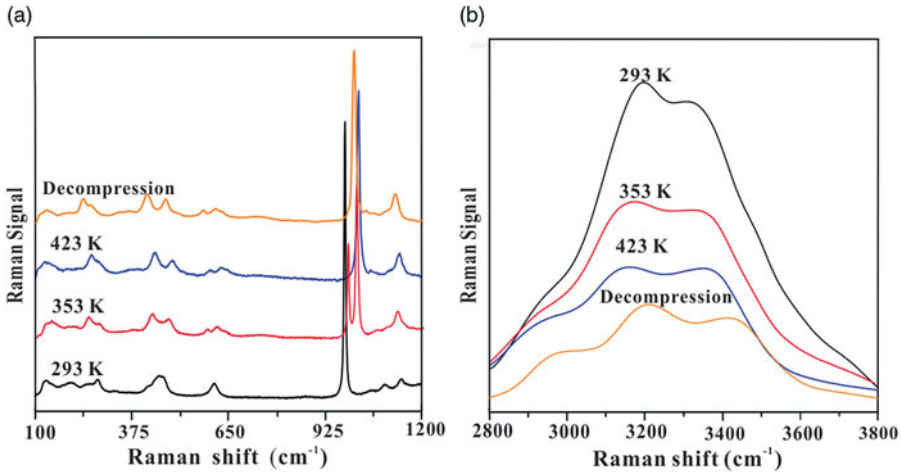

Figure 6. Raman spectra of chalcanthite at 2.9 GPa and 293–423 K. The variation of the vibrational modes of (a) sulfate anion and (b) water molecule. (Operating conditions: excitation laser power 20 mW.). K–Temperature (Kelvin).

When the temperature was increased to 353 K, one clear new peak appeared at 1007 cm^{-1}. This Raman peak became stronger with increasing temperature and eventually replaced the original ν_1 (SO_4) mode at 983 cm^{-1}. Two corresponding peaks were formed by splitting of the ν_2 (SO_4) peak at 460 cm^{-1} and ν_4 (SO_4) peak at 610 cm^{-1}, respectively. Chang and Huang[17] suggested the splitting of the chalcanthite Raman peaks indicates a dehydration reaction at atmospheric pressure. The appearance of new peaks can provide robust evidence for the dehydration of chalcanthite ($CuSO_4{\cdot}5H_2O$) to bonattite ($CuSO_4{\cdot}3H_2O$). The dehydration reaction of chalcanthite occurred at 353 K and 2.9 GPa. The splitting of ν_2 (SO_4) at 460 cm^{-1} and ν_4 (SO_4) at 610 cm^{-1} still occurs when the pressure and temperature revert to ambient condition.

In Fig. 6(b), the total curve is too flat at a relatively low temperature of 293 K. With increasing temperature, the peak at 2964 cm^{-1} became increasingly clear and eventually evolved into a shape similar to the shoulder in the Raman spectrum after dehydration. The ν_1 (H_2O) and ν_3 (H_2O) peaks both became weaker with increasing temperature. The initial band at 3154 cm^{-1} exhibited a blue shift and a wider FWHM, and the band at 3274 cm^{-1} became broader and shifted to the lower–frequency range. As in the study of atmospheric-pressure dehydration of chalcanthite performed by Chang and Huang,[17] the variations of Raman modes of H_2O were applied to extrapolate the occurrence of sample dehydration. The results show that the Raman modes of H_2O and SO_4^{2-} change simultaneously during the dehydration reaction of chalcanthite. In Fig. 6(b), three peaks can still be clearly seen for the recovered sample after decompression. Similar variations in the of Raman modes at 5.8 GPa were also observed before and after dehydration experiments, as shown in Fig. 7. The dehydration reaction is accompanied by a structural phase transition from the original chalcanthite ($CuSO_4{\cdot}5H_2O$) to bonattite ($CuSO_4{\cdot}3H_2O$). This structural phase transition is irreversible because the crystal structure completely changes from the triclinic to the monoclinic crystallographic system before and after dehydration. This differs from the reversible phase transitions at high pressure and room temperature, which are caused by pressure-induced distortion of the crystalline structure of chalcanthite. The dehydration temperatures obtained from the Raman spectra were 353 K at 2.9 GPa and 503 K at 5.8 GPa.

Impedance spectroscopy of chalcanthite at high pressure and high temperature

The electrical conductivity of chalcanthite was measured in the temperature range 293–673 K at 3.2 and 6.2 GPa, the results are shown in Fig. 8. The impedance spectroscopy consisted of a semi-circular arc at high frequencies and a straight line at low frequencies. The fitted equivalent circuit and the method used for electrical conductivity calculations were similar to those described above for the experiments at room temperature and high pressure.

The electrical conductivity results acquired from the impedance spectroscopy were used to investigate the relationship between the electrical conductivity of chalcanthite and reciprocal temperature, the results are shown in Fig. 9. Based on the slope of the linear relationship, the activation enthalpy can be made out by virtue of Arrhenius relation. Variations in the activation enthalpy can provide valuable clues to the occurrence of dehydration reactions of hydrous minerals at high temperatures and high pressures.[29] At 323 and at 523 K, the onset temperatures for chalcanthite dehydration, the relationship became discontinuous. At 3.2 GPa the activation enthalpy increased from 0.190 ± 0.002 eV in the temperature range 293–323 K to 0.203 ± 0.004 eV in the temperature range 373–498 K. At 6.2 GPa the activation enthalpy increased from 0.132 ± 0.003 eV in the temperature range 293–523 K to 0.390 ± 0.002 eV in the temperature range 553–673 K. Such clear electrical conductivity discontinuities can be used to deduce dehydration of chalcanthite.

Dehydration significantly changed the electrical conductivity of chalcanthite. The temperature ranges (323–373 K for 3.2 GPa and 523–553 K for 6.2 GPa) determined from our electrical conductivity results are close to the dehydration temperatures obtained from the high-temperature Raman

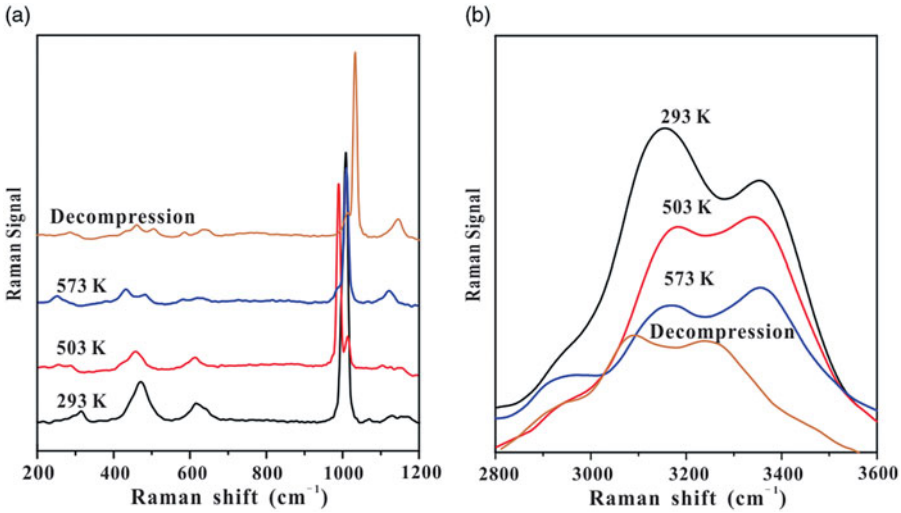

Figure 7. Raman spectra of chalcanthite at 5.8 GPa and 293–573 K. The variation of the vibrational modes of (a) sulfate anion and (b) water molecule. (Operating conditions: excitation laser power 20 mW.) K–Temperature (Kelvin).

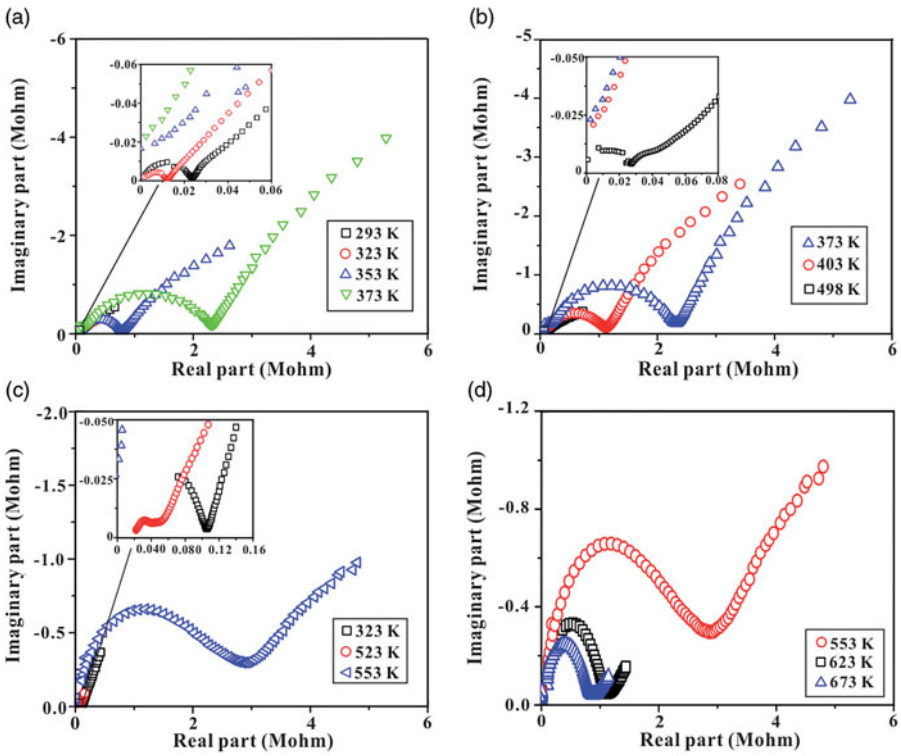

Figure 8. Representative complex spectra of the sample at high temperatures and high pressures. (a) and (b) A series of impedance spectra of chalcanthite at temperature range from 293 to 498 K and 3.2 GPa. (c) and (d) A series of impedance spectra of chalcanthite at temperature range from 323 to 673 K and 6.2 GPa. (Operating conditions: signal voltage 1 V; scanning frequency range 10^{-1} to 10^{7} Hz). K–Temperature (Kelvin).

spectra (353 K for 2.9 GPa and 503 K for 5.8 GPa). The same heating rate was used in all experiments, therefore, it can be deduced that the dehydration temperature of chalcanthite increases with increasing pressure. The linear fits can be described as

$$T(\mathrm{K}) = 200 + 50P(\mathrm{GPa}) \quad (2)$$

This positive correlation between dehydration temperature and pressure is similar to those observed for other hydrous minerals such as blodite [$Na_2Mg(SO_4)_2{\cdot}4H_2O$],[30] and can be attributed to the pressure-dependent interaction of hydrogen bonding for water molecules. An increase in pressure changes the distances among the sulfate tetrahedra, copper ions, and water molecules, and further affects the interactions of hydrogen bonding, especially at high-temperature conditions.

Conclusions

The *in situ* phase stability and dehydration of chalcanthite were investigated at high-temperature and high-pressure ranges, i.e. 293–693 K and 1.0–24.0 GPa, using a diamond anvil cell. At ~7.3 GPa, a secondary phase transition was

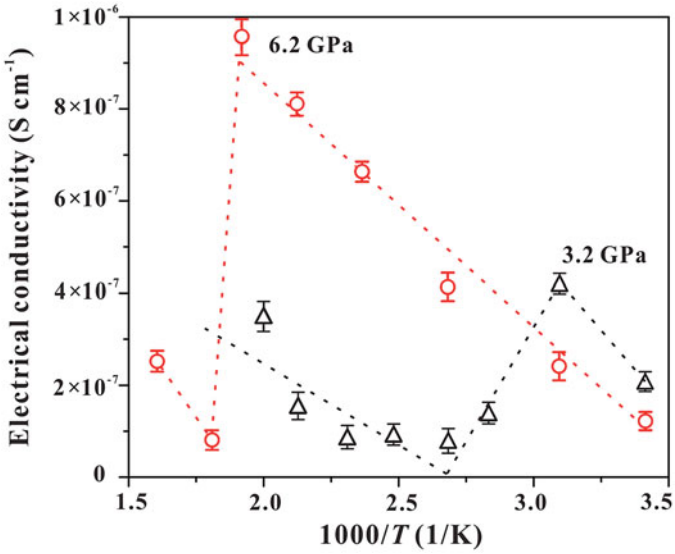

Figure 9. Relationship between electrical conductivity and reciprocal temperatures for chalcanthite under conditions of 3.2 and 6.2 GPa. *T*–absolute temperature; K–Temperature (Kelvin), and S–Siemens.

determined on the basis of the discontinuous variations in the electrical conductivity and Raman full-width at half maximum for ν_1 (H_2O) mode at room temperature. At ~10.3 GPa, another secondary phase transition was confirmed by virtue of the disappearance of the ν_1 (SO_4), ν_3 (SO_4) and ν (Cu–O) modes and the discontinuities of ν_1 (SO_4), ν_2 (SO_4), ν_4 (SO_4), ν_1 (H_2O), and ν_3 (H_2O) modes in Raman shifts and full-width at half maximum at ambient temperature. Based on the analysis of high-temperature and high-pressure Raman spectra and electrical conductivity, the dehydration temperature of chalcanthite increased from ~350 to ~500 K at elevated pressures of ~3.0 and ~6.0 GPa, respectively. Our obtained results reveal that the dehydration temperature of chalcanthite increases with increasing pressure. The positive effect of pressure on the dehydration temperature for chalcanthite is attributed to the pressure-dependent interaction of hydrogen bonding for water molecules.

Funding

This research was financially supported by the Strategic Priority Research Program (B) of the Chinese Academy of Sciences (XDB 18010401), Key Research Program of Frontier Sciences of CAS (QYZDB-SSW-DQC009), "135" Program of the Institute of Geochemistry of CAS, Hundred Talents Program of CAS and NSF of China (41474078, 41774099 and 41772042).

References

[1] Saig, A.; Danon, A.; Finkelstein, Y.; Kimmel, G.; Koresh, J. A Continuous Polymorphic Transition of Coordinating Water Molecules in $CuSO_4·5H_2O$. *Journal of Physics and Chemical of Solids* **2003**, *64*, 701–706.

[2] Beevers, C.; Lipson, H. The Crystal Structure of Copper Sulphate Pentahydrate, $CuSO_4·5H_2O$. *Proceedings of the Royal Society of London* **1934**, *146*, 570–582.

[3] Berger, J. Infrared and Raman Spectra of $CuSO_4$, $5H_2O$; $CuSO_4$, $5D_2O$; and $CuSeO_4$, $5H_2O$. *J. Raman Spectrosc.* **1976**, *5*, 103–114.

[4] Höfer, S.; Popp, J.; Mayerhöfer, T. Determination of the Dielectric Tensor Function of Triclinic $CuSO_4·5H_2O$. *Vibrational Spectroscopy* **2013**, *67*, 44–54.

[5] Huang, E.; Xu, J.; Lin, J.; Hu, J. Pressure–Induced Phase Transitions in gypsum. *High Pressure Research* **2000**, *17*, 57–75.

[6] Brand, H.; Fortes, A.; Wood, I.; Vocadlo, L. Equation of State and Pressure–Induced Structural Changes in Mirabilite ($Na_2SO_4·10H_2O$) Determined from ab Initio Density Functional Theory Calculations. *Physics and Chemicals of Minerals* **2010**, *37*, 265–282.

[7] Gromnitskaya, E.; Yagafarov, O.; Lyapin, A.; Brazhkin, V.; Wood, I.; Tucker, M.; Fortes, A. The High–Pressure Phase Diagram of Synthetic Epsomite ($MgSO_4·7H_2O$ and $MgSO_4·7D_2O$) from Ultrasonic and Neutron Powder Diffraction Measurements. *Physics and Chemicals of Minerals* **2013**, *40*, 271–285.

[8] Beevers, C.; Lipson, H. Crystal Structure of Copper Sulphate. *Nature* **1934**, *133*, 215–215.

[9] Bacon, G.; Curry, N. The Water Molecules in $CuSO_4·5H_2O$. *Proceeding of the Royal Society of London* **1962**, *266*, 95–108.

[10] Bacon, G.; Titterton, D. Neutron–Diffraction Studies of $CuSO_4·5H_2O$ and $CuSO_4·5D_2O$. *Zeitschrift Für Kristallographie–Crystalline Materials* **1975**, *141*, 330–341.

[11] Liu, D.; Ullman, F. Raman Spectrum of $CuSO_4·5H_2O$ Single Crystal. *Journal of. Raman Spectroscopy* **1991**, *22*, 525–528.

[12] Fu, X.; Yang, G.; Sun, J.; Zhou, J. Vibrational Spectra of Copper Sulfate Hydrates Investigated with Low–Temperature Raman Spectroscopy and Terahertz Time Domain Spectroscopy. *Journal of Physical Chemistry A* **2012**, *116*, 7314–7318.

[13] Sun, W.; Dai, L.; Li, H.; Hu, H.; Jiang, J.; Hui, K. Effect of Dehydration on the Electrical Conductivity of Phyllite at High Temperatures and Pressures. *Mineralogy and Petrology* **2017**, *111*, 853–863.

[14] Hicks, T.; Secco, R. Dehydration and Decomposition of Pyrophyllite at High Pressures: Electrical Conductivity and X–Ray Diffraction Studies to 5 GPa. *Canadian Journal of Earth Science* **1997**, *34*, 875–882.

[15] Mirwald, P. Experimental Study of the Dehydration Reactions Gypsum–Bassanite and Bassanite–Anhydrite at High Pressure: Indication of Anomalous Behavior of H_2O at High Pressure in the temperature range of 50–300 °C. *The Journal of Chemical Physics* **2008**, *128*, 074502.

[16] Nandi, P.; Deshpande, D.; Kher, V. Dehydration Steps in $CuSO_4·5H_2O$ crystals. *Proceedings of the Indian Academy of Sciences–Chemical Sciences* **1979**, *88*, 113–124.

[17] Chang, H.; Huang, P. Dehydration of $CuSO_4·5H_2O$ Studied by Thermo–Raman Spectroscopy. *Journal of the Chinese Chemical Society* **1998**, *45*, 59–66.

[18] White, R. Variable Temperature Infrared Study of Copper Sulfate Pentahydrate Dehydration. *Thermochimica Acta* **2012**, *528*, 58–62.

[19] Dai, L.; Wu, L.; Li, H.; Hu, H.; Zhuang, Y.; Liu, K. Evidence of the Pressure–Induced Conductivity Switching of Yttrium–Doped $SrTiO_3$. *Journal of Physics: Condensed Matter* **2016**, *28*, 475501.

[20] Dai, L.; Zhuang, Y.; Li, H.; Wu, L.; Hu, H.; Liu, K.; Yang, L.; Pu, C. Pressure–Induced Irreversible Amorphization and Metallization with a Structural Phase Transition in arsenic telluride. *Journal of Materials Chemistry C* **2017**, *5*, 12157–12162.

[21] Dai, L.; Liu, K.; Li, H.; Wu, L.; Hu, H.; Zhuang, Y.; Yang, L.; Pu, C.; Liu, P. Pressure–Induced Irreversible Metallization Accompanying the Phase Transitions in Sb_2S_3. *Physical Review B* **2018**, *024103*.

[22] Dai, L.; Wu, L.; Li, H.; Hu, H.; Zhuang, Y.; Liu, K. Pressure–Induced Phase–Transition and Improvement of the Microdielectric Properties in yttrium–doped $SrZrO_3$. *Europhysics Letters* **2016**, *114*, 56003.

[23] Reddy, B.; Sreerasmulu, P.; Ramesh, K.; Reddy, Y. Electron–Paramagnetic Resonance of Cu (II) and

Vibrational–Spectrum of Chalcanthite. *Anales De La Asociacion Quimica Argentina* **1988**, *76*, 297–302.

[24] Bouchard, M.; Smith, D. Catalogue of 45 Reference Raman Spectra of Minerals Concerning Research in Art History or Archaeology, Especially on Corroded Metals and Coloured Glass. *Spectrochimica Acta Part A: Molecular and Biomolecular Spectroscopy* **2003**, *59*, 2247–2266.

[25] Hayez, V.; Guillaume, J.; Hubin, A.; Terryn, H. Micro–Raman Spectroscopy for the Study of Corrosion Products on Copper Alloys: Setting up of a Reference Database and Studying Works of Art. *Journal of Raman Spectroscopy* **2004**, *35*, 732–738.

[26] Makreski, P.; Jovanovski, G.; Dimitrovska, S. Minerals from Macedonia XIV. Identification of Some Sulfate Minerals by. *Vibrational (Infrared and Raman) Spectroscopy. Vibrational Spectroscopy* **2005**, *39*, 229–239.

[27] Murugan, R.; Ghule, A.; Chang, H. Thermo–Raman Spectroscopic Studies on Polymorphism in Na_2SO_4. *Journal of Physics: Condensed Matter* **2000**, *12*, 677–700.

[28] Velde, B. Effect of Pressure on OH–Stretching Frequencies in kaolinite and ordered aluminous serpentine. *American Mineralogist* **1984**, *66*, 196–200.

[29] Hu, H.; Dai, L.; Li, H.; Hui, K.; Sun, W. Influence of Dehydration on the Electrical Conductivity of Epidote and Implications for High Conductivity Anomalies in subduction zones. *Journal of Geophysical Research: Solid Earth* **2017**, *122*, 2751–2762.

[30] Comodi, P.; Stagno, V.; Zucchini, A.; Fei, Y.; Prakapenka, V. The Compression Behavior of Blödite at Low and High Temperature up to ~10 GPa: Implications for the Stability of Hydrous Sulfates on Icy Planetary Bodies. *Icarus* **2017**, *285*, 137–144.